DISCLAIMER

This report was prepared as an account of work sponsored by an agency of the United States Government. Neither the United States Government nor any agency thereof, nor any of their employees, makes any warranty, express or implied, or assumes any legal liability or responsibility for the accuracy, completeness, or usefulness of any information, apparatus, product, or process disclosed, or represents that its use would not infringe privately owned rights. Reference herein to any specific commercial product, process, or service by trade name, trademark, manufacturer, or otherwise does not necessarily constitute or imply its endorsement, recommendation, or favoring by the United States Government or any agency thereof. The views and opinions of authors expressed herein do not necessarily state or reflect those of the United States Government or any agency thereof. Reference herein to any social initiative (including but not limited to Diversity, Equity, and Inclusion (DEI); Community Benefits Plans (CBP); Justice 40; etc.) is made by the Author independent of any current requirement by the United States Government and does not constitute or imply endorsement, recommendation, or support by the United States Government or any agency thereof.

A DOE Energy Innovation Hub

SCALE MG Cross Section Processing for High Void BWR Using the AMPX 1,597-group Library

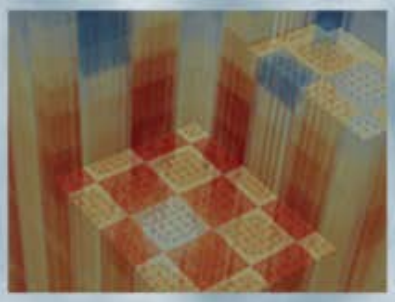

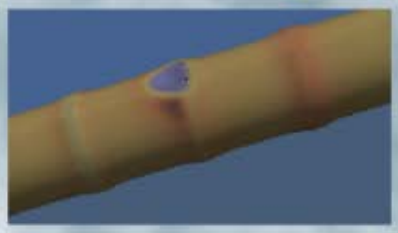

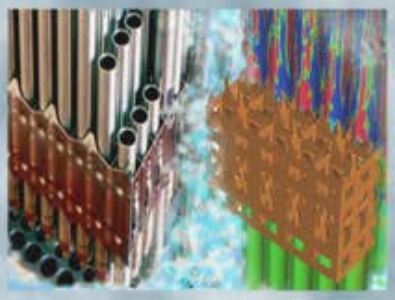

Revision 0

Byoung-kyu Jeon
Won Sik Yang
University of Michigan

Kang Seog Kim
Kevin Clarno
Oak Ridge National Laboratory

Sep 28, 2018

U.S. DEPARTMENT OF ENERGY | Nuclear Energy

REVISION LOG

Revision	Date	Affected Pages	Revision Description
0	9/28/2018	All	Initial version

Export Controlled None

IP/Proprietary/NDA Controlled None

Sensitive Controlled None

Unlimited All Pages

Requested Distribution:

To: N/A

Copy: N/A

Reviewed by:

Date:

Reviewer:

EXECUTIVE SUMMARY

The CASL VERA neutronic simulator MPACT has been developed by Oak Ridge National Laboratory (ORNL) and University of Michigan for the pressurized water reactor applications. The MPACT capability is being extended for the boiling water reactor (BWR) analysis. Recent investigation showed that the MPACT multigroup (MG) library has limitations for high void BWR fuels because of the very coarse group structure. Since the MPACT MG library is generated with the AMPX/SCALE code package developed at ORNL, enhancement of the AMPX/SCALE code package and its MG library must be preceded to improve the accuracy of the MPACT MG library. Therefore, a new 1597-group structure was developed and an AMPX 1597-group library was generated. This ultra-fine group (UFG) library resulted in significant improvements in accuracy for fast spectrum systems compared to the AMPX 252-group results. However, the use of the AMPX 1597-group library requires significantly increased burden on memory and computing time.

The purpose of this study is to enhance the computational efficiency of the lattice calculation with the AMPX 1597-group library without loss of accuracy. A new two-step procedure has been proposed to enhance the computational efficiency; (1) UFG calculations are first performed for unit cells or with a low order solver, and then (2) the UFG cross sections are collapsed into coarse group cross sections with which lattice transport calculations are to be performed. Benchmark results show that the new two-step procedure with the AMPX 1597-group library results in significant improvements in reaction rates compared to the AMPX 252-group library while reducing the computing time significantly compared for to the single-step UFG lattice calculation, for example by a factor of 13 times for a 9x9 BWR assembly with 99% void fraction.

As an extra work, the AMPX/SCALE code package with the AMPX 1597-group library was applied to fast reactor analysis because neutron spectra of the high void BWR fuels are similar to those of fast reactor systems. Detailed reaction rate analysis was performed for various fast reactor fuels and simple 3D whole-core calculation was performed by using TWODANT to consider neutron leakage and the core simulator, DIF3D/VARIANT.

TABLE OF CONTENTS

FIGURES

TABLES

ACRONYMS

1D	one-dimensional
2D	two-dimensional
ABTR	Advanced Burner Test Reactor
ANL	Argonne National Laboratory
AMPX	resonance processing code; the name is no longer an acronym
BWR	boiling water reactor
CASL	Consortium for Advanced Simulation of Light Water Reactors
CE	continuous energy (as in cross sections)
CENTRM	Continuous ENergy Transport Module
CMFD	Coarse Mesh Finite Difference
DIF3D	Code System Using Variational Nodal Methods and Finite Difference Methods to Solve Neutron Diffusion and Transport Theory Problems
ENDF	Evaluated Nuclear Data File
FDM	Finite Difference Method
LANL	Los Alamos National Laboratory
LWR	Light Water Reactor
NEWT	New ESC-based Weighting Transport code
MCNP	Monte Carlo N-Particle code
MC^2-3	Multigroup Cross section generation Code for fast reactor analysis
MG	multi-group (as in cross sections)
MOC	Method of Characteristic
MPACT	radiation transport code; the name is no longer an acronym
MSR	Molten Salt Reactor
NR	narrow resonance
ORNL	Oak Ridge National Laboratory
PW	pointwise
PWR	pressurized water reactor
RR	resolved resonance
SCALE	Standardized Computer Analyses for Licensing Evaluations
TWODANT	TWO-dimensional Diffusion-Accelerated Neutral particle Transport
VARIANT	VARIational Anisotropic Nodal Transport solver
VERA	Virtual Environment for Reactor Applications
UFG	ultrafine group (as in cross sections)
URR	unresolved resonance
XS	cross section
XSDRN	One-dimensional discrete-ordinates code

1. INTRODUCTION

The CASL VERA neutronics simulator MPACT [Mpa13] is being developed by Oak Ridge National Laboratory (ORNL) and University of Michigan for various reactor applications. The MPACT and simplified MPACT cross section libraries have been developed in 51- and 252-group structures for the MPACT neutron transport calculations by using the AMPX [Wia14] and SCALE [Sca16] code packages developed at ORNL. It has been noted that the conventional AMPX/SCALE procedure has limited applications for highly voided BWR fuels because of its poor accuracy in unresolved and fast energy regions. Detailed investigation [Jeo18] found that the poor accuracy of the AMPX/SCALE procedure is mainly due to the normalization error of probability table in unresolved resonance (URR) energy region and the inaccurate modeling of broad scattering resonances of intermediate weight nuclides in a 51- or 252-group structure. In addition, a large reactivity error was also introduced by the un-shielded (n,p) cross section of Cl^{35}. Recent improvements [Kim18] on AMPX-based probability tables and self-shielding of Cl^{35} have reduced significantly the reactivity bias observed for BWR and MSR pin cell problems. It was also shown that a new ultra-fine group (UFG) AMPX library prepared in a 1,585-group structure could yield remarkable improvements in reaction rates and reactivity even for a 99% voided BWR pin cell problem.

However, a lattice calculation in UFG level is computationally very expensive. To reduce the computational time of the UFG lattice calculation without loss of accuracy, a two-step UFG lattice calculation was proposed. In this procedure, a low order UFG transport calculation is first performed and the UFG cross sections are condensed into an intermediate group (i.e., 252). Then, the lattice calculation is performed in an intermediate group level. In order to test the proposed two-step lattice calculation, a new UFG AMPX library was generated in a 1,597-group structure rather than the preliminary 1,585-group structure to comply with the boundary of current 252-group structure. To cover a wide range of reactor application, UFG transport calculations are performed for unit cells in thermal spectrum problems to consider local heterogeneity effects or for simplified assembly models of fast spectrum problems to account for anisotropic scattering and leakage effects. Pin cell and lattice benchmark results indicate that the two-step approach enhances the applicability of the AMPX/SCALE system to the highly voided BWR problem without a noticeable increase in computational time.

To extend the applicability of the AMPX/SCALE system to fast spectrum systems, a new procedure to generate region-dependent broad-group cross sections has been developed by adopting TWODANT [Alc90], which was developed by Los Alamos National Laboratory (LANL). In this procedure, to account for the region-to-region spectral transition, a whole-core TWODANT calculation are performed in cylindrical-z geometry using homogenized assembly cross sections in the UFG group structure, and then the UFG group cross sections are collapsed into broad group cross sections using the TWODANT solution. A new utility code, AMPX_ISOTXS, has been developed to convert resulting the AMPX/SCALE MG cross sections into the ISOTXS format, and to condense UFG cross sections to broad group for those code systems. The whole core simulation was

performed using the DIF3D/VARINAT [Pal95] code system, which was developed by Argonne National Laboratory (ANL). Preliminary verification tests of new fast spectrum analysis procedure with AMPX/SCALE MG cross sections has been performed using a simplified mini core model derived from the Advanced Burner Test Reactor (ABTR) design [Cha06].

The purpose of this report is to document the performance of two-step cross section generation approach using the new UFG AMPX/SCALE library for highly voided BWR and the fast reactor applications. Detailed methodologies and procedures for the two-step calculation are also included in this report. Following is the summary of this document:

- Generation of the new 1,597-group AMPX MG libraries (Chapter 2),
- Brief methodologies and procedures of the two-step cross section generation procedure using the 1,597-group AMPX MG libraries (Chapter 2),
- Benchmark calculations and reaction rate analysis using the current 252-group AMPX libraries and the collapsed 252-group cross sections generated by two-step procedure (Chapter 3),
- Description of the new fast reactor analysis procedure using the 1,597-group AMPX MG libraries (Chapter 4),
- Performance of the new fast reactor analysis procedure (Chapter 4).

2. AMPX/SCALE MG CROSS SECTION PROCESSING PROCEDURES

A new AMPX 1,597-group library was generated using the AMPX-6 and SCALE code packages to comply with the current AMPX 56- and 252-group libraries. To enhance the efficiency of lattice transport calculation with the AMPX 1,597-group library, a two-step cross section processing procedure has been developed and implemented in SCALE. The methodologies and procedure to generate the AMPX 1,597-group library and intermediate group cross sections are discussed in this chapter.

2.1 LIBRARY GENERATION AND CROSS SECTION PROCESSING PROCEDURES

AMPX-6 is a code package to generate the AMPX MG and CE cross section libraries for SCALE and MPACT by processing the ENDF/B libraries. The AMPX MG library includes resonance self-shielding factors called Bondarenko F-factors, principle cross sections and scattering matrices for all the ENDF/B nuclides along with fundamental control data. In the standard SCALE MG procedure, the AMPX MG master library is converted into the problem dependent AMPX MG working library by using several SCALE modules. Figure 2.1.1 [Kim16] provides the standard SCALE procedure to process problem dependent MG cross sections and scattering matrices. BONAMI calculates self-shielded cross sections for all energy groups and nuclides based upon the Bondarenko approach. Then CENTRM performs the PW slowing down calculations for resolved resonance and thermal energy ranges, which are coupled with the MG fixed source calculations for fast and very low energy groups. The MG cross sections for the PW energy range in CENTRM are obtained by flux weighting, and they replace the BONAMI based cross sections to enhance accuracy. This standard SCALE MG procedure has been used in this study.

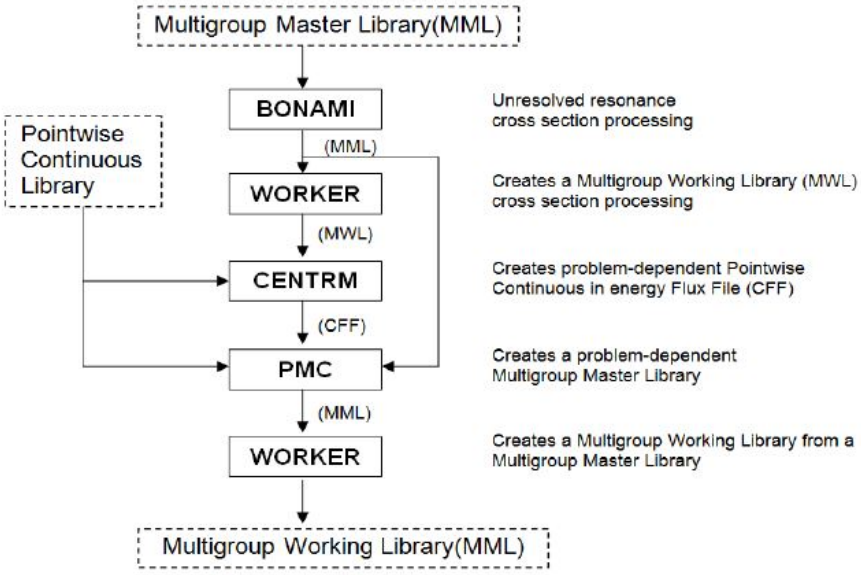

Figure 2.1.1 Sequence to generate the AMPX MG working library

Currently the SCALE 6.2 and the development version include the AMPX 56- and 252-group libraries. To improve the accuracy of AMPX/SCALE procedure for fast spectrum applications, the number of group structure was preliminarily increased from 252-group to 1,585-group by combining MC^2-3 UFG and SCALE 252-group structures [Jeo18]. However, the 1,585-group structure does not comply with the current 252-group structure because of the direct use of MC^2-3 UFG structure at high energy range. In addition, the 1,585-group AMPX master library only includes 33 major isotopes which was used for preliminary benchmark calculations. Therefore, New AMPX 252- and 1,597-group libraries have been generated for most isotopes in ENDF/B VII.1 and tested with various benchmark problems in this report. Table 2.1.1 illustrates the group structure of the AMPX 1,597-group master library and Tables 2.1.2 provides the detailed information for the SCALE code package and AMPX MG master libraries used in this report. Note that the previous issues [Jeo18] on probability tables for the URR region and self-shielding of Cl^{35} were fixed in the new AMPX 252- and 1,597-group libraries in Table 2.1.2.

Table 2.1.1 Group Structure of the 1,597-group AMPX master library

Energy Range (MeV)	# of groups	Self-shielding treatment
10^{-11} ~ 10^{-9}	5	Bondarenko approach
10^{-9} ~ 10^{-4}	155	CENTRM PW calculation (up to URR boundary)
10^{-4} ~ 20.0	1,437	Bondarenko approach (from URR energy range)

Table 2.1.2 SCLAE and AMPX MG libraries

Program	Location
[Jupiter.ornl.gov]	
1,597G AMPX library	/home/hbq/nrc_vfg/results/nr_master/nr_std_flux_master_ss103
252G AMPX library	/home/f78/ampx_2018/input-e71-252g-lwr/ffactors/heterogenous/lib252_VII.1-Het-Ffactors-withRemoval-293K-cl35mt103
SCALE6.3 beta1	/home/flj/scale_dev_release/build/first/INSTALL/bin/scale

2.2 DEVELOPMENT OF TWO-STEP CROSS SECTION GENERATION PROCEDURE

To enhance the lattice calculation accuracy without increasing the computational time significantly, the two-step lattice calculation capability with an internal energy group collapsing has been implemented to the AMPX/SCALE MG cross section generation procedure. In the standard SCALE procedure, XSPROC module of SCALE generates a problem-dependent 1,597-group AMPX working library by using BONAMI and CENTRM as described in Section 2.1. To perform internal group collapsing of problem-dependent 1,597-group AMPX working library, several existing transport solvers in SCALE code package were invoked. Selection of transport solver is mainly determined by the target problem, since characteristics of fast spectrum reactor are totally different from that of thermal reactor.

In fast reactor system, the local heterogeneity effect is less important, and the reflector effect is more pronounced due to the much longer neutron mean free path (~10 cm), compared to PWR (~1 cm) [Yan12]. Long mean free path also results in global coupling, and thus the spectral transition from region to region is important when generating the broad group cross section in fast reactor system. Anisotropic scattering, inelastic scattering and (n, 2n) reactions also increase noticeably at high energy range. For these reasons, a whole core transport calculation with homogenized assemblies and higher order scattering treatment is generally performed for fast spectrum reactors, while repeated unit cell transport calculations with explicit geometry and lower order scattering treatment are used for thermal spectrum reactors. The two-step cross section generation procedure was prepared in both ways to cover a wide range of reactor applications by using existing transport solvers (1D XSDRN, 2D NEWT) in the SCALE code package.

In the SCALE code package, the problem dependent MG cross section libraries can be generated by multiple XSPROC sequences (e.g. CSAS-MG, T-XSEC, CSASI etc.) for use in later transport calculations [SCA12]. Each sequence uses different processing procedures and provides different type of libraries. To generate the collapsed cross section for individual nuclides, the CSAS-MG sequence, which provides self-shielded cross sections of the individual nuclides using the standard SCALE procedure, was used in this study. Figure 2.2.1 shows the computational flow of two-step lattice calculation based on the CSAS-MG sequence. The unit cell based two-step procedure offers three calculation options (0D slowing down, 1D XSDRN and 2D NEWT) to obtain the cell-weighted collapsing spectrum, and two options (2D FDM and 2D NEWT) are available for assembly-based procedure. Table 2.2.1 briefly describes characteristics of each solver available in both two-step cross section generation procedures. It is noted that Coarse Mesh Finite Difference (CMFD) acceleration routine in NEWT was also invoked as 0D slowing down and 2D FDM solvers for internal group collapsing.

In the unit cell based procedure, 0D slowing down is the most efficient approach to determining the slowing down spectra of target problem. The treatment of higher order scattering also can be considered further by using the P_N approximation. However, the current 0D slowing down solver in two-step procedure was limited to the diffusion theory of CMFD solver. 1D XSDRN and 2D NEWT are alternative options to resolve errors

caused by the neglect of space-dependent neutron distribution, though those options require more computation resources. This MG cross section generation approach based on the detailed spectrum calculation for specific homogenized composition of unit cell, which was initially proposed by ANL and widely used for fast reactor analysis through various codes, such as MC^2-3 [Lee11] and ECCO [Rim95].

In the assembly based procedure, 2D FDM and 2D NEWT solvers were used to take into account the leakage effect from neighboring cells. Since the main objective of two-step procedure is to reduce the computational burden of lattice transport calculation, 2D NEWT transport solver was used only to obtain the reference lattice solution in this report. As shown in the Table 2.2.1, 2D NEWT provides more rigorous solutions, compared to 2D FDM solver. However, this approach is particularly useful for the treatment of anisotropic scattering, but not sufficiently efficient for use in homogenized lattice cross section generation. It is well known that the importance of anisotropic scattering increases above 100 keV [Yan10]. Due to the presence of small amount of water in BWR, the fluxes above 100 keV in highly voided BWR is much less than the those of fast reactor. This indicates that the higher order anisotropic scattering treatment is relatively less important in highly voided BWR, compared to fast reactor system. It was also reported that the diffusion theory with transport corrected cross section generally works well in the assembly calculation even with the 80% void fraction [Tak06]. Thus, 2D FDM is a proper choice of internal collapsing solver for two-step BWR lattice calculation with high void fraction. In addition, FDM generally requires fine mesh size comparable to neutron mean free path to obtain reliable flux spectra. Because of relatively large mean free path in highly voided BWR, FDM calculation can be performed with a coarse meth, which reduces the computing time noticeably.

Table 2.2.1 Comparison of transport solvers in two-step procedure

Characteristics	Slowing down	XSDRN	NEWT	FDM
Dimension (Coordinate)	0D	1D (cylindrical)	2D (XY)	2D (XY, XZ)
Anisotropic scattering	-	√	√	-
Leakage effect	-	-	√	√
Computing time	A few secs[a]	< 10 secs[a]	A few mins[a] / ~2 hours[b]	< a min[b]

[a] computing time for a unit cell
[b] computing time for the BWR 9 by 9 lattice problem

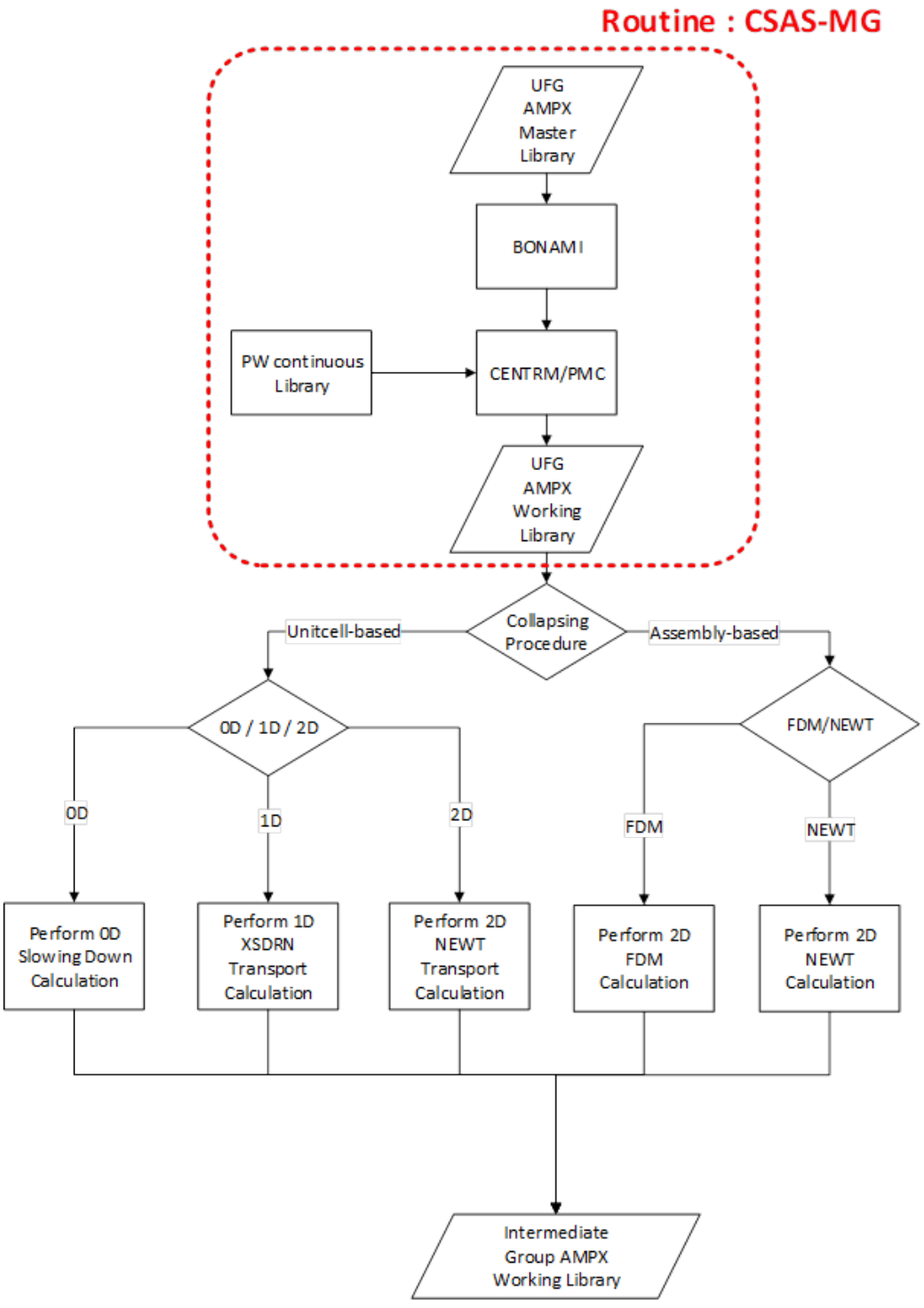

Figure 3.0.1 Computational flow of two-step cross section generation procedure

3. BENCHMARK TESTS

To examine the performance of two-step MG cross section generation procedure for various cases, six pin cell and one lattice benchmark problems were developed including a typical PWR UO_2 fuel pin, two BWR UO_2 fuel pins with 90% and 99% void fractions, a simplified ABTR fuel pin, homogenized MSR and MET-1000 fuels, and a BWR lattice problem with a 99% void fraction. Table 3.0.1 provides the brief description of pin cell benchmark problems. More detailed information can be found in Reference [Aki02] for the PWR and BWR problems, in [Cha06] for ABTR, in [Tau80] for MSR, and in Reference [Kim18] for MET-1000, respectively. The BWR lattice problem is a 9 by 9 BWR fuel assembly design based on Reference [Aki02], which has five different types of fuel rods with different U^{235} enrichments varying from 3.0 wt. % to 6.3 wt. %. The isotopic composition and geometrical configuration of the 99% BWR fuel assembly are presented in Table 3.0.3 and Figure 3.0.1, respectively. All the benchmark problems were simulated using a square pin cell geometry of MG-KENO. Each MG-KENO simulation was performed with 150 active cycles and 100,000 histories per cycle. Note that Zr^{90} was not used in these benchmark problems except for ABTR pin cell problem, since a significant cross section error was found in Zr^{90} at the vicinity of lower boundary of URR in the new 252- and 1,597-group libraries as observed in the old 252-group library. Detailed description of this error was summarized in Section 4.2. It is also noted that non-negligible discrepancy was observed in a verification test of the current XSDRN group collapsing routine against MCNP6.

Using the new 1,597-group AMPX master libraries, collapsed 252-group cross sections were prepared by the two-step procedure, while the original 252- and 1,597-group cross sections were generated using the standard SCALE procedure as shown in Figure 2.1.1. The self-shielded cross sections in the resolved resonance and thermal regions were regenerated using the 2D method of characteristic (MOC) option of CENTRM except for MSR and MET-1000, for which the infinite homogeneous medium option was used. The isotopic composition of the ABTR, MSR and MET-100 fuels are shown in Table 3.0.2. It is noted that higher order scattering matrices were collapsed using the scalar flux rather than the higher flux moments in these benchmark tests.

Table 3.0.1 Pin cell benchmark problems

Fuel	Case	^{235}U w/o	Temperature (K)			Void %
			Fuel	Clad	Moderator	
PWR	A	6.5	900	600	600	0%
	B1		900	600	600	90%
	B2		900	600	600	99%
ABTR	C	-	300	300	300	-
MSR	D	-	300			-
MET-1000	E	-	300			

Table 3.0.2 Isotopic composition for fast reactor problems C, D and E

ABTR			Homogenized MSR		Homogenized MET-1000	
Region	**Nuclide**	**Number density**	**Nuclide**	**Number density**	**Nuclide**	**Number density**
Fuel	92235	3.2247E-05	92235	3.1000E-05	92235	3.1000E-05
	92238	2.0222E-02	92238	4.2750E-03	92238	4.2750E-03
	94239	3.4991E-03	94239	4.0400E-04	94239	4.0400E-04
	94240	3.7398E-04	94240	5.4000E-05	94240	5.4000E-05
	40090	3.7526E-03	94241	2.7000E-05	94241	2.7000E-05
Bond	11023	2.2272E-02	94242	5.4000E-05	94242	5.4000E-05
Cladding	26054	4.0824E-03	11023	5.3830E-03	11023	5.3830E-03
	26056	6.4085E-02	17035	1.5010E-02	17035	1.5010E-02
Coolant	11023	2.2272E-02	17037	4.8332E-03	17037	4.8332E-03

Table 3.0.3 Isotopic compositions of BWR fuel assembly with 99% void fraction

Type	**Fuel 1**	**Fuel 2**	**Fuel 3**	**Fuel 4**	**Fuel Gd**	**Moderator / Water Rod**	
Temp	**900K**					**600K**	
Nuclide	**Number density**					**Nuclide**	**Number density**
U^{235}	1.432E-03	1.137E-03	9.094E-04	6.820E-04	1.039E-03	H^{1}	4.932E-04
U^{238}	2.103E-02	2.132E-02	2.155E-02	2.177E-02	1.949E-03	O^{16}	2.466E-04
O^{16}	4.493E-02	4.492E-02	4.492E-02	4.491E-02	4.399E-03	-	
Gd^{154}	-				4.186E-05		
Gd^{155}					2.874E-04		
Gd^{156}					3.995E-04		
Gd^{157}					3.060E-04		
Gd^{158}					4.854E-04		
Gd^{160}					4.309E-04		
Zr^{91}	4.8280E-3						
Zr^{92}	7.3713E-3						
Zr^{94}	7.5006E-3						
Zr^{96}	1.2070E-3						

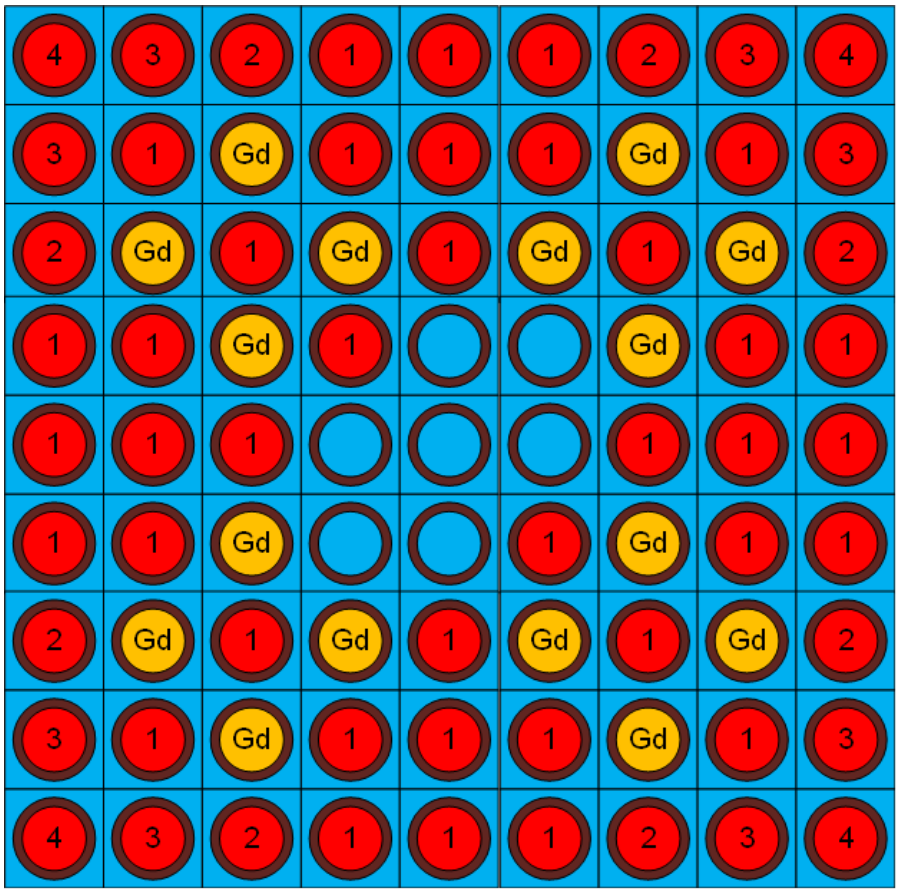

Figure 3.0.1 Geometrical configuration of BWR fuel assembly

3.1 EIGENVALUE BENCHMARK RESULTS

Pin cell benchmark calculations were performed using the SCALE MG-KENO module with the ENDF/B-VII.1 AMPX 252- and 1,597-group libraries. The calculations were also performed with the collapsed 252-group cross sections, which were generated by using 0D slowing down and 2D NEWT calculations. As mentioned above, 1D XSDRN solver was not used due to a problem in its group collapsing routine. The reference solutions were obtained by performing CE MCNP calculations with 1,000 active cycles and 100,000 histories per cycle to yield relative errors of reaction rates less than 0.3%. Figure 3.1.1 shows a comparison of 252-group neutron spectra for the cases, A through E. As discussed in Section 2.2, it can be clearly seen that the fluxes above 100 keV in highly voided BWR is less than those of ABTR and MSR.

The BWR lattice problem was also simulated by using the SCALE MG-KENO and 2D NEWT modules with the ENDF/B-VII.1 1,597-group libraries and the 252-group cross sections collapsed with 2D FDM and NEWT solutions. NEWT calculations were performed with P_3 anisotropic scattering treatment for fuels and P_1 for structural materials and water. Note that CMFD acceleration was not used in the NEWT calculations and four

meshes per pin cell were used in 2D FDM calculation. The CE MCNP solution for the BWR lattice was also obtained with 1,000 active cycles and 100,000 histories per cycle.

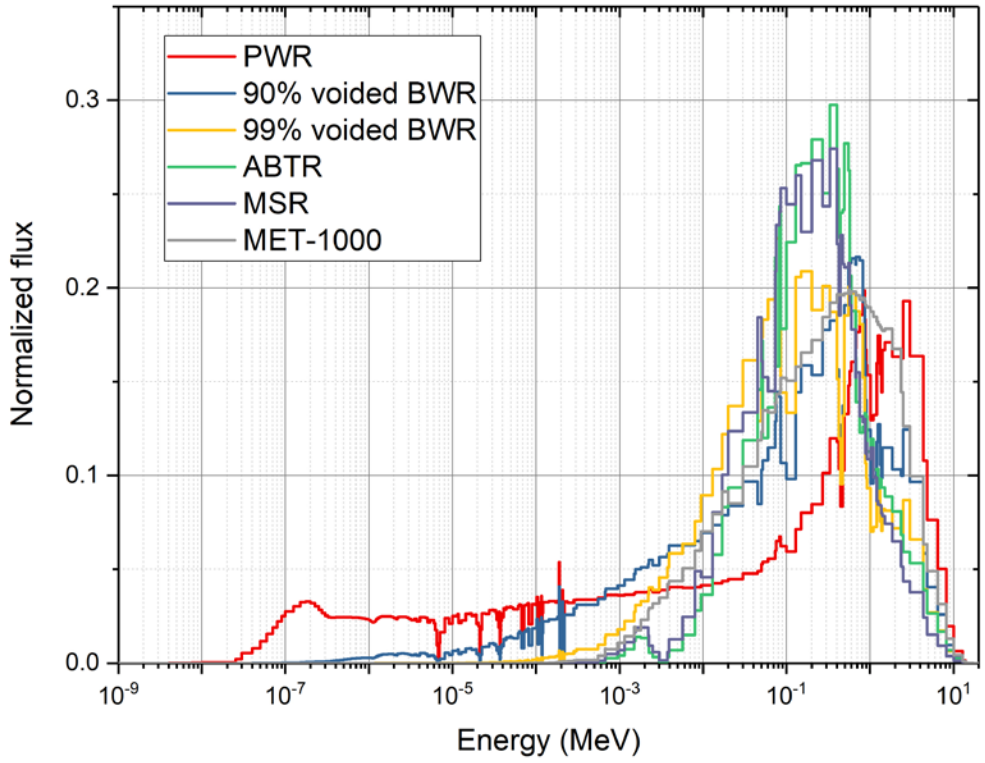

Figure 3.1.1 252-group fluxes in fuel for various pin cell benchmark problems

Table 3.1.1 compares the MG-KENO and MCNP eigenvalue results obtained with the 252- and 1,597-group AMPX libraries. The maximum eigenvalue differences between the MCNP and MG-KENO results are -597 and -217 pcm for the AMPX 252- and 1,597-group libraries, respectively. The results with 1,597-group library generally agree well with the MCNP results. The 252-group results are also comparable to the MCNP results except for the ABTR and 99% voided BWR lattice problems. For example, the MSR result with 252-group library shows good agreement with the MCNP result, even slightly better than the 1,597-group result. However, the previous investigation [Jeo18] showed that there might be a huge error cancellation, which leads to the good eigenvalue agreements. Furthermore, huge errors observed in the ABTR and BWR lattice problems indicate that the current 252-group AMPX MG library may not be applicable to the analysis of the fast spectrum problems. Note that U^{235} cross sections and poor thermal scattering matrices at thermal groups are the primary error sources for the PWR problem A [Kim17].

Table 3.1.2 demonstrates the performance of two-step procedure. MG-KENO solutions with the collapsed 252 group cross sections agree very well with the reference 1,597-group MG-KENO solutions except for the PWR case with the 0D slowing down solver. As mentioned in Section 2.2, the 0D slowing down solver has a drawback to represent space-dependent within cell spectra, which leads to -268 pcm difference in eigenvalue for the PWR problem. To address the error cancellation in the multiplication factor obtained with

the current 252-group cross section library and to quantify the improvements in reaction rates by adopting the two-step procedure, detailed reaction rate analysis results are discussed in the next section. It was also found that the BWR lattice solutions with the 252 group cross sections collapsed with the slowing down and NEWT solutions agree well with the reference solution obtained without the intermediate step calculation. The eigenvalue difference between the results obtained with the collapsed 252- and the 1,507-group cross sections are -19 pcm for 2D FDM and -3 pcm for 2D NEWT, respectively.

Table 3.1.1 Eigenvalue results of MG-KENO and MCNP6 for various pin cell problems

Fuel	Case	Multiplication factor (k_{inf})				
		MCNP	MG-KENO			
			252-group	Δk (pcm)	1,597-group	Δk (pcm)
PWR	A	1.42901 (6)	1.42710 (16)	-191 (17)	1.42684 (16)	-217 (17)
BWR	B1	1.00449 (4)	1.00376 (13)	-73 (14)	1.00372 (11)	-77 (11)
	B2	0.90253 (4)	0.90323 (10)	70 (10)	0.90242 (19)	9 (10)
ABTR	C	1.60150 (4)	1.59553 (10)	-597 (11)	1.59990 (10)	-160 (11)
MSR	D	1.13927 (1)	1.13943 (6)	16 (6)	1.13896 (7)	-31 (7)
MET-1000	E	2.22385 (2)	2.22248 (11)	-137 (11)	2.22251 (9)	-134 (9)
BWR Lattice	-	0.77481 (1)	0.77750 (10)	269 (11)	0.77454 (9)	-27 (10)

Table 3.1.2 Eigenvalue results of MG-KENO with the collapsed 252-group cross sections for various benchmark problems

Fuel	Case	Multiplication factor (k_{inf})				
		1,597-group MG-KENO	MG-KENO (collapsed 252-group)			
			Slowing down	Δk (pcm)	NEWT	Δk (pcm)
PWR	A	1.42684 (16)	1.42416 (21)	-268 (26)	1.42623 (16)	-61 (26)
BWR	B1	1.00372 (11)	1.00344 (10)	-28 (15)	1.00352 (14)	-20 (18)
	B2	0.90242 (19)	0.90265 (9)	23 (12)	0.90246 (10)	4 (14)
ABTR	C	1.59990 (10)	1.59998 (11)	8 (15)	1.59978 (12)	-12 (16)
MSR	D	1.13896 (7)	1.13872 (6)	-24 (10)	1.13879 (7)	-17 (10)
MET-1000	E	2.22251 (9)	2.22240 (14)	-11 (17)	2.22247 (15)	-4 (18)
BWR Lattice	-	0.77454 (9)	0.77435[a] (8)	-19 (12)	0.77451 (8)	-3 (12)

[a] Collapsed with 2D FDM solution

The pin-by-pin fission power distributions of MCNP6 and 1,597-group NEWT calculations are compared in Figure 3.1.2. The power distribution obtained by NEWT agrees well with the reference solution within a maximum error of -1.937%. Relatively large errors are observed in the fuel pins with gadolinium, where the escape probability of neutrons deviates substantially from the average value due to the strong absorber. In the standard SCALE procedure, a heterogeneous lattice is approximately represented by a one group parameter, Dancoff factor, assuming the repeated unit cell geometry [Sca16]. Therefore, the inaccuracy of pin-power around strong absorber can be further improved by employing more detailed multi-group escape cross sections derived from the whole lattice

calculation. Figure 3.1.3 compares the NEWT pin power distributions obtained with the original 1,597-group cross sections and the 252-group cross sections collapsed with the FDM solution. The power distribution obtained with the two-step lattice calculation is in good agreement with the 1,597-group result within a maximum error of 1.242% at the periphery. The computing times for the 252-group and 1,597-group NEWT calculations are 440 seconds and 1.75 hours, respectively. The computing time for internal group collapsing with the 2D FDM calculation is only 33 seconds. These results indicate that the two-step lattice calculation significantly improves the computation efficiency by a factor of 13 for the lattice problem without loss of accuracy.

0.410	0.296	0.309				0.338	0.303	0.402
0.383	0.373	-1.937			0.378	-1.886	0.377	0.406
0.521	-1.888	0.356	-1.905	0.327	-1.882	0.380	-1.846	0.502
0.515	0.322	-1.877	0.377	0.312	0.398	-1.860	0.353	0.479
0.601	0.484	0.540	0.378	0.424	0.383	0.491	0.450	0.608

Figure 3.1.2 Comparison of pin-by-pin fission power distribution between 1,597-group NEWT and MCNP6 for 99% voided BWR lattice problem (180˚ symmetry)

-0.338	-0.251	-0.408				-0.408	-0.251	-0.338
-0.304	-0.251	0.294			-0.504	0.283	-0.233	-0.286
0.009	0.467	-0.216	0.294	-0.408	0.283	-0.198	0.479	0.051
0.659	0.136	0.467	-0.251	-0.251	-0.233	0.479	0.145	0.684
1.242	0.659	0.009	-0.286	-0.338	-0.286	0.051	0.684	1.182

Figure 3.1.3 Comparison of pin-by-pin fission power distribution between 1,597-group NEWT and NEWT with collapsed 252-group cross sections for 99% voided BWR lattice problem (180˚ symmetry)

3.2 REACTION RATE ANALYSIS

The benchmark results in Sections 3.1 show that the MG-KENO multiplication factors obtained with the current AMPX 252-group library and the collapsed 252-group cross sections generally agree well with the MCNP results except for the ABTR and BWR lattice results obtained with the current 252-group library. However, the good multiplication factor results might be due to error cancellations, and hence more detailed analysis is required to quantitatively evaluate the quality of the MG cross sections.

In order to identify the main error sources and the degree of error cancellation of the observed eigenvalue difference between MG-KENO and MCNP results, detailed reaction rate analyses were performed. The reaction rate differences between MG-KENO and MCNP and their contributions to the reactivity difference were estimated for each nuclide and each energy group as follows:

a. Perform the CE MCNP calculation and tally the MG scalar fluxes, isotopic capture and fission reaction rates, and average number of neutrons released per fission ($\bar{\upsilon}$) in addition to eigenvalue.
b. Perform the standard SCALE MG-KENO calculation to obtain the parameters in the step a.
c. Calculate the contribution to the reactivity difference of the reaction rate difference (i.e., due to cross section and flux errors) for each nuclide, reaction type, and energy group using the following formula:

$$\Delta\rho^{k'}_{c,g',i'} = \frac{N^{k'}_{i'}(\sigma^{k'}_{c,g',i'}\phi_{g',i'} - \hat{\sigma}^{k'}_{c,g',i'}\hat{\phi}_{g',i'})V_{i'}}{\sum_i\sum_k\sum_g N^k_i \upsilon^k_{g,i}\sigma^k_{fis,g,i}\phi_{g,i}V_i}, \tag{3.2.1}$$

$$\Delta\rho^{k'}_{fis,g',i'} = \frac{1}{k_\infty} - \frac{\sum_i\sum_k\sum_g N^k_i(\sigma^k_{a,g,i} - \sigma^k_{n,2n,g,i} - 2\sigma^k_{n,3n,g,i})\phi_{g,i}V_i}{\sum_i\sum_k\sum_g N^k_i \upsilon^k_{g,i}\sigma^k_{fis,g,i}\phi_{g,i}V_i - N^{k'}_{i'}\upsilon^{k'}_{g',i'}(\sigma^{k'}_{fis,g',i'}\phi_{g',i'} - \hat{\sigma}^{k'}_{fis,g',i'}\hat{\phi}_{g',i'})V_{i'}} + \frac{N^{k'}_{i'}(\sigma^{k'}_{fis,g',i'}\phi_{g',i'} - \hat{\sigma}^{k'}_{fis,g',i'}\hat{\phi}_{g',i'})V_{i'}}{\sum_i\sum_k\sum_g N^k_i \upsilon^k_{g,i}\sigma^k_{fis,g,i}\phi_{g,i}V_i - N^{k'}_{i'}\upsilon^{k'}_{g',i'}(\sigma^{k'}_{fis,g',i'}\phi_{g',i'} - \hat{\sigma}^{k'}_{fis,g',i'}\hat{\phi}_{g',i'})V_{i'}}, \tag{3.2.2}$$

where $\Delta\rho^{k'}_{x',g',i'}$ is the reactivity difference due to the difference in the fission ($x = fis$) or capture ($x = c$) reaction rate of nuclide k' in group g' and region i'. N^k_i is the number density of nuclide k in region i, and V_i is the volume of region i. A quantity with caret (^) symbol indicates the cross section or flux from MG-KENO, while the other quantities are from MCNP. Multiplication factor (k_∞) in Eq. (3.2.2) can be estimated by using the following equation:

$$k_{\infty} = \frac{\sum_i \sum_k \sum_g N_i^k \upsilon_{g,i}^k \sigma_{fis,g,i}^k \phi_{g,i} V_i}{\sum_i \sum_k \sum_g N_i^k (\sigma_{a,g,i}^k - \sigma_{n,2n,g,i}^k - 2\sigma_{n,3n,g,i}^k) \phi_{g,i} V_i}. \quad (3.2.3)$$

Table 3.2.1 demonstrates the reaction rate analysis results obtained with Eq. (3.2.1) and (3.2.2). The detailed description of each column was described in the foot notes of Table 3.2.1. The reactivity differences determined from two eigenvalues calculated using the tallied reaction rates with Eq. (3.2.3) are consistent with the simulated reactivities. As mentioned in Section 3.1, the detailed reaction rate analysis reveals that the good eigenvalue agreements in Table 3.1.1 are due to the error cancellation among absorption and fission reactions of different nuclides. It can be seen from Table 3.2.1 that the collapsed 252-group cross section improved reaction rates significantly. However, it is still possible that the good eigenvalue agreements are due to error cancellation among energy groups. Thus, the differences in group-wise reaction rates were also examined.

Table 3.2.1 Reaction rate analysis results for 99% voided BWR, ABTR and MSR

Case	$\Delta\rho_{252g}^{a}$ [pcm]	$\Delta\rho_{col}^{b}$ [pcm]	Nuclide	Current 252-group			Collapsed 252-group (NEWT)		
				RR_{cap}^{c}	RR_{fis}^{c}	SUM	RR_{cap}^{c}	RR_{fis}^{c}	SUM
B2 (99% BWR)	121	-8	92235	22	-57	120	-1	-1	-4
			92238	114	63		26	-30	
			8016	-10	-		-1	-	
			13027	-12	-		1	-	
C (ABTR)	-223	-54	92235	-1	1	-221	0	0	-50
			92238	-189	32		-22	0	
			94239	-116	66		-4	-7	
			94240	-8	6		-1	0	
			40090	-5	-		-8	-	
			11023	-8	-		-3	-	
			26054	-2	-		0	-	
			26056	-6	-		-6	-	
D (MSR)	8	-30	92235	2	-3	7	0	-1	-28
			92238	66	49		5	-8	
			94239	1	-4		-19	0	
			94240	2	5		0	-1	
			94241	-1	6		5	-5	
			94242	-4	4		0	0	
			11023	-1	-		0	0	
			17035	-117	-		-11	0	
			17037	-1	-		1	0	

[a,b] Reactivity difference determined from two eigenvalues deduced from reaction rates with Eq. (3.2.3) with 252-group library and collapsed 252-group cross section, respectively.

[c] $RR_{cap} = \sum_g \Delta\rho_{c,g}^k$, $RR_{fis} = \sum_g \Delta\rho_{fis,g}^k$ determined from Eq. (3.2.1) and (3.2.2)

To investigate the group-wise contributions to the observed differences in reactivity and reaction rates, the MG-KENO and MCNP results were examined in more detail. Figures

3.2.1 through 3.3.7 show the reactivity differences in group-wise reaction rates for each nuclide and reaction of three problems in Table 3.2.1. Figures 3.2.1 and 3.2.2 compare the reactivity error caused by the reaction rate error of each nuclide and reaction for the 99% voided BWR problem obtained with the 252-group AMPX library and the collapsed 252-group cross sections, respectively. Similar comparisons are presented in Figures 3.2.3 to 3.2.6 for major actinides of the ABTR and MSR problems, and in Figure 3.2.7 for Cl^{35} absorption of the MSR problem. As shown in Figures 3.2.1, 3.2.3, and 3.2.5, the BWR and fast reactor problems show noticeable discrepancies in the actinide reaction rates in high energy groups. These discrepancies are consistent with the results in the previous analysis [Jeo18], which is caused by the limitation of the Bondarenko approach in the 252-group structure.

The reaction rate analysis results with the collapsed 252-group cross sections in Figures 3.2.2, 3.2.4, 3.2.6, and 3.2.7 clearly show the performance of the two-step procedure on reaction rates. For example, the maximum group-wise reactivity error due to U^{238} capture reaction error was reduced from -410 to 13 pcm for the B2 case, from 180 to 22 pcm for the C case, and 350 pcm to 5 pcm for the D case. The reactivity error in the MSR due to Pu^{239} fission reaction error is also reduced from -220 to -4 pcm. Furthermore, there is still noticeable reactivity difference due to the Cl^{35} absorption in the current 252-group library despite of self-shielded (n,p) cross section, whereas the errors have been eliminated by using the two-step procedure as shown Figure 3.2.7. Note that remaining 20 pcm error of ABTR result around 100 keV is due to the cross section difference of Zr^{90}, which is described in Section 4.2. These results indicate that the two-step procedure improves not only eigenvalues, but also group-wise reaction rates significantly at high energy range.

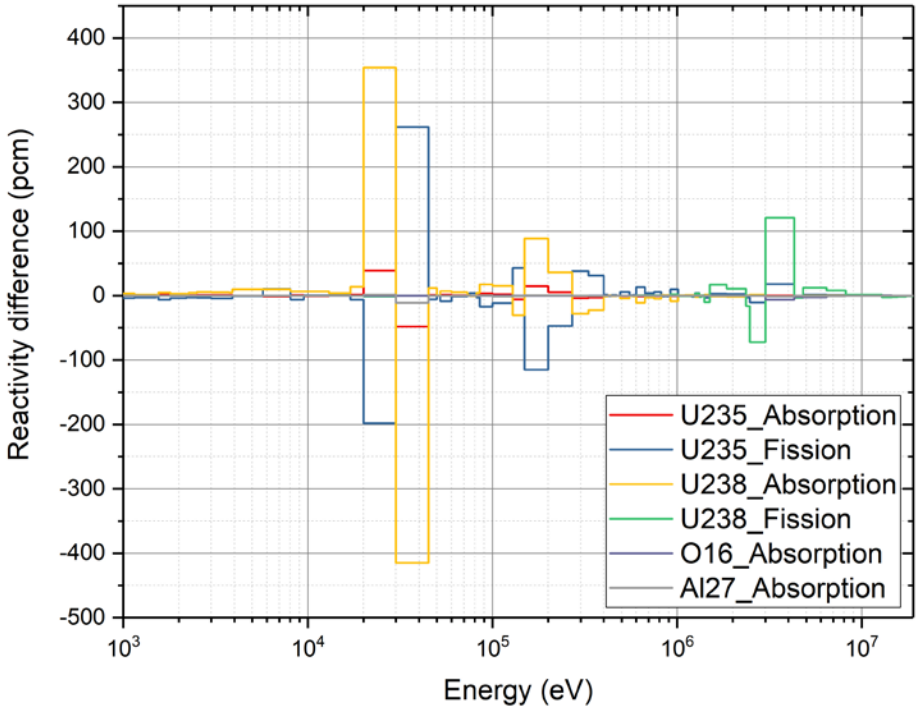

Figure 3.2.1 Reactivity differences with current 252-group library for 99% voided BWR problem

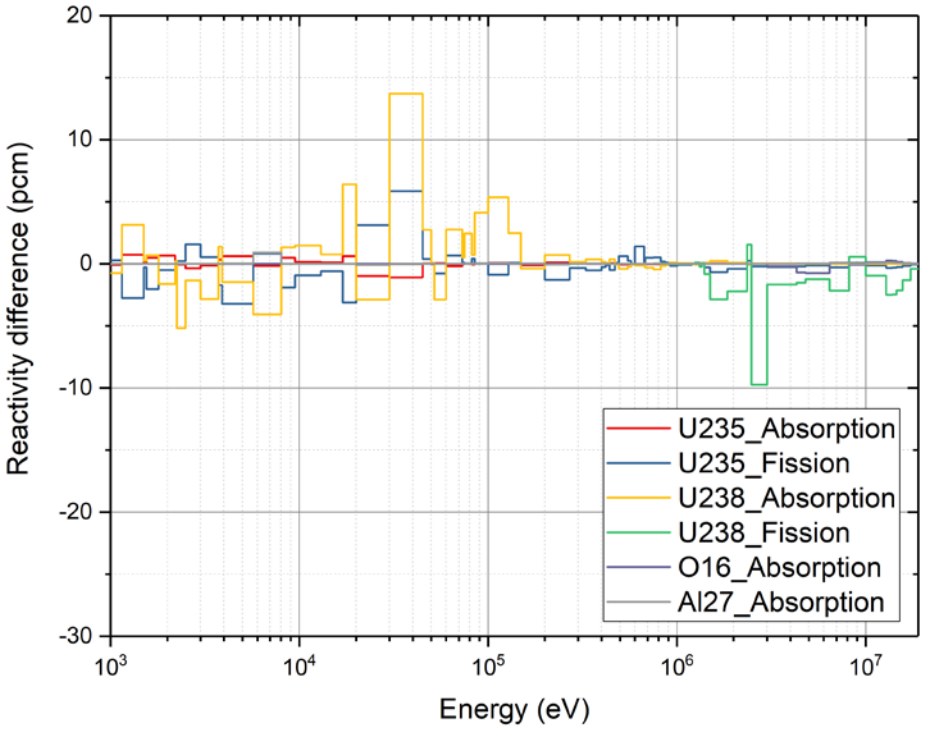

Figure 3.2.2 Reactivity differences with collapsed 252-group cross section for 99% voided BWR problem

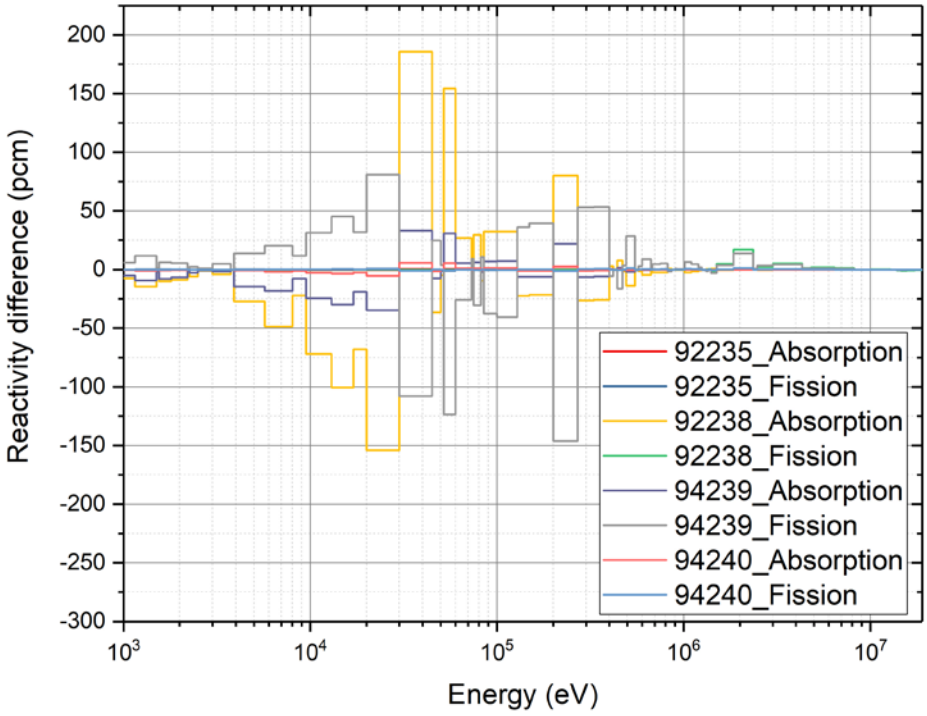

Figure 3.2.3 Reactivity differences with current 252-group library for ABTR problem

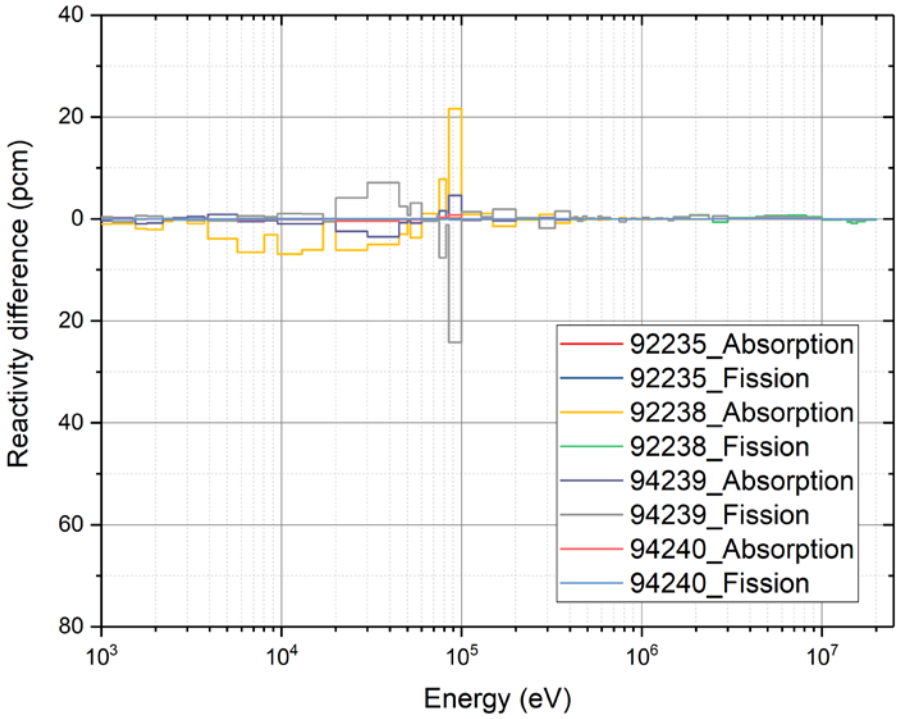

Figure 3.2.4 Reactivity differences with collapsed 252-group cross sections for ABTR problem

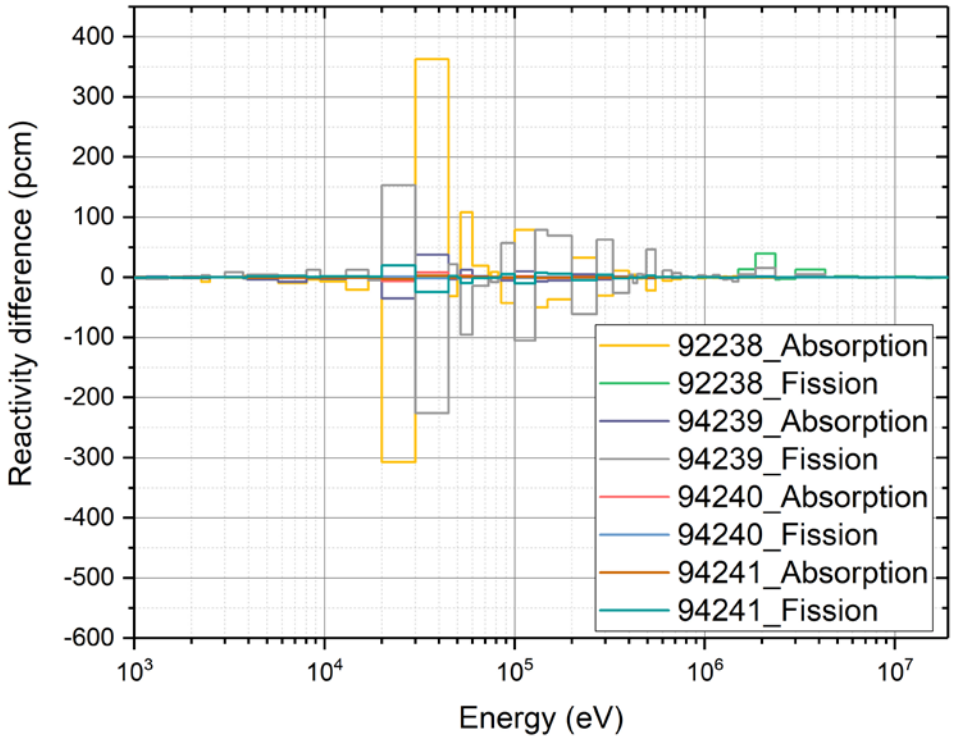

Figure 3.2.5 Reactivity differences with current 252-group library for MSR problem

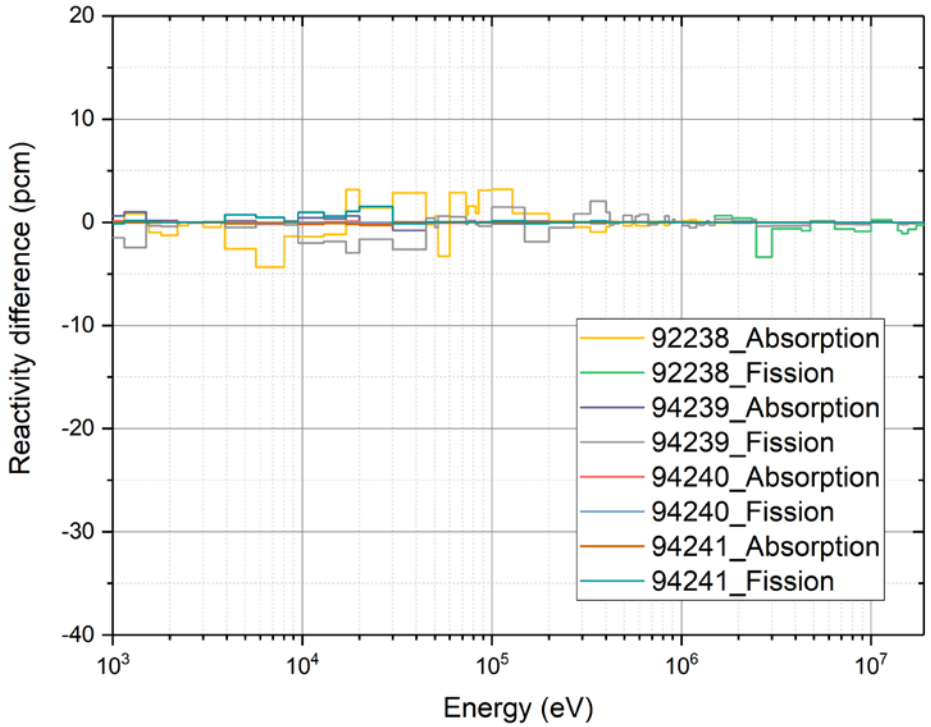

Figure 3.2.6 Reactivity differences with collapsed 252-group cross sections for MSR problem

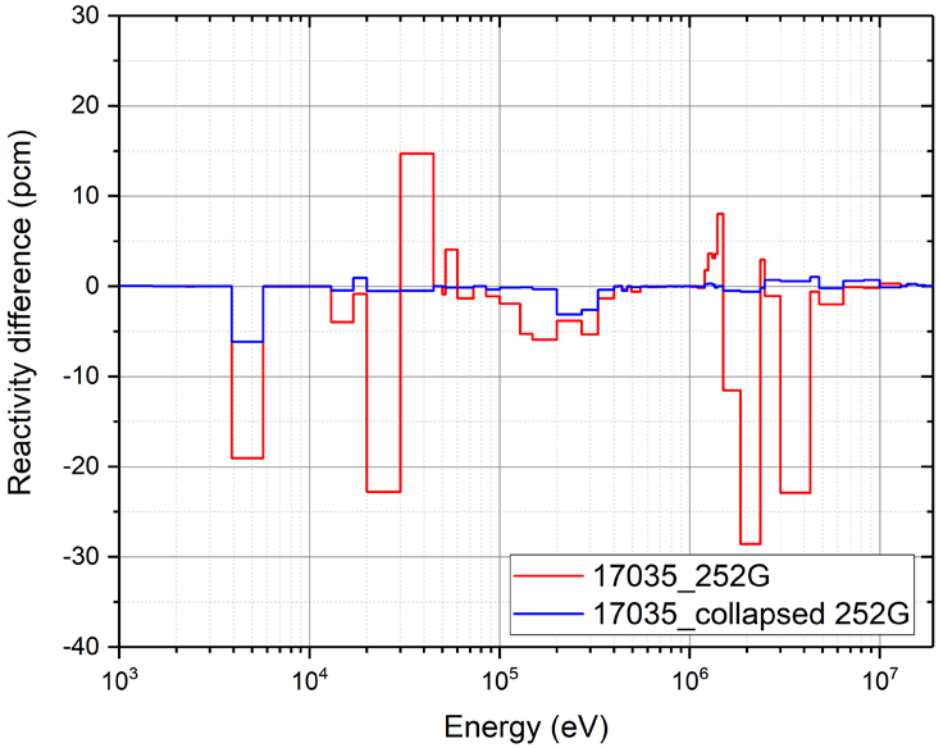

Figure 3.2.7 Comparison of reactivity differences due to Cl^{35} absorption with current 252g library and collapsed 252-group cross sections for MSR problem

4. FAST REACTOR ANALYSIS WITH AMPX/SCALE MG LIBRARIES

In Section 3, it was observed that the AMPX/SCALE code package with the new 1597-group library is applicable to not only BWR problem but also fast reactor pin cell and homogenized assembly problems. It was also observed that the assemby-based two-step procedure with the 2D FDM solver noticeably enhances the efficiency of lattice calculation without loss of accuracy for highly voided BWR. However, the assembly-based two-step procedure in Section 2.2 cannot be directly applicable to fast reactor core analysis due to the neglect of higher order anisotropic scattering in the 2D FDM calculation and the limitation of current SCALE code package to model the whole core geometry. Since broad group cross sections for fast reactor core are generally space-dependent, they are typically determined in two steps using a transport solver with simplified whole core geometry.

In the fast reactor analysis procedure of ANL, UFG or intermediate group macroscopic cross sections are first generated by MC^2-3 [Lee11] for each homogenized composition for all unique fuel, plenum, shielding, and reflector regions. Then, using these composition-dependent macroscopic cross sections, a TWODANT whole-core transport calculation is performed in cylindrical-z (R-Z) geometry to determine the region-wise flux spectra that will be used in generating region-dependent broad group cross sections [Yan10]. These broad group cross sections are used in subsequent whole core and fuel cycle analyses. Now the AMPX/SCALE code package has a capability to generate UFG or intermediate group macroscopic cross sections for homogenized pin cells and assemblies using the two-step procedure, and thus the AMPX/SCALE cross section generation procedure can be extened further to fast reactor core analysis by adopting the ANL procedure.

Figure 4.0.1 shows the new fast reactor analysis procedure with AMPX/SCALE MG processing. For a detailed region-to-region spectral transition calculation with higher order scattering treatment, a TWODANT transport calculation is performed with the 1,597-group AMPX library. An in-house utility code, named AMPX_ISOTXS, has been developed to convert AMPX MG cross sections into the ISOTXS format for TWODANT calculation, to read region-dependent flux spectra from the TWODANT solution, and to generate the region-dependent broad group cross sections in the ISOTXS format for the subsequent whole core analysis using the ANL's DIF3D/VARIANT code system.

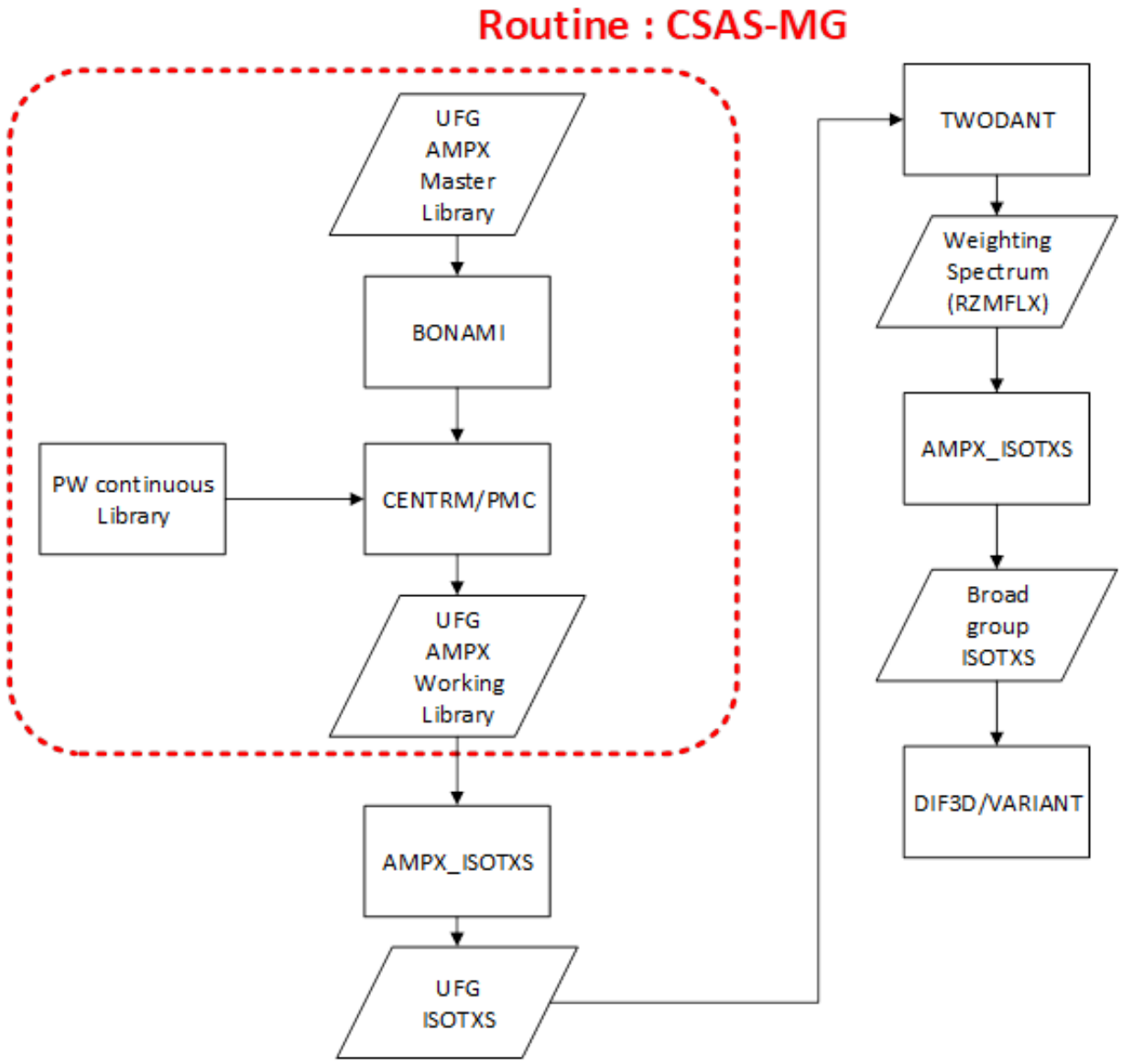

Figure 4.0.1 Fast reactor analysis procedure with AMPX/SCALE MG processing

4.1 SIMPLIFIED ABTR MINI CORE PROBLEM BENCHMARK TEST

For a preliminary verification of the newly implemented SCALE MG cross section processing capability for fast reactor analysis, a simplified mini-core benchmark problem, has been developed from the ABTR core benchmark problem by reducing the number of assemblies and isotopes. The core has 19 driver fuel assemblies, 72 radial reflector assemblies, and 36 barrel assemblies representing the core barallel and surrounding sodium. The assembly pitch is 14.685 cm, the active core height is 84.4 cm. Table 4.1.1 and Figure 4.1.1 show the isotopic compositions and the radial core configuration, respectively. The reference solution was obtained by performing a CE MCNP calculation with 2,000 active cycles and 100,000 histories per cycle. A set of AMPX/SCALE 33-group broad group cross sections were prepared by performing a TWODANT transport calculation with homogenized assembly compositions and the 1,597-group AMPX library. For comparison, a set of 33-group cross sections was also prepared using the MC^2-3 code. It is noted that the 2,082-group cross section library of MC^2-3 is based on the ENDF/VII.0 data while the AMPX/SCALE and MCNP cross sections are based on the ENDF/VII.1 data. In the TWODANT calculation, 1.5 cm spatial mesh interval was used. A scattering order of P_5 was used in both TWODANT and DIF3D/VARIANT calculations.

The transport calculation results for the ABTR mini-core problem are shown in Table 4.1.2. The eigenvalue difference between MC^2-3/VARIANT and MCNP is -12,504 pcm for P_1 scattering approximation, and it reduces to -134 pcm for P_5 scattering. As mentioned in Section 2.2, this is because the anisotropic scattering effect is more pronounced in fast reactors. Although MC^2-3 cross sections are based on the ENDF/B VII.0 and the AMPX/SCALE cross secrions are based on the ENDF/B-VII.1, similar trends are observed for both DIF3D/VARIANT results. However, the AMPX/SCALE 33-group cross section resulted in non-negligible eigenvalue differeces even with P_5 scattering order, compared to the MCNP result. It was found that some structural materials caused noticeable biases on reactivity. As an example, when substantial amounts of Cr^{52} and Fe^{56} were added to fuel driver, the VARIANT results with the AMPX/SCALE cross sections increased the deviation in k_∞ from -324 pcm to -890 pcm. Furthermore, the difference in k_∞ between the VARIANT results obtained with MC^2-3 and AMPX/SCALE cross sections increases as the scattering order increases. For example, it is -51 pcm for P_1 scattering approximation but increases to -190 pcm for P_5 scattering. This suggests that the higher order scattering matrices as well as principal cross sections of some structural materials are the sources for the observed reactivity deviations. To identify the error sources of the multiplication factor, cross sections and scattering matrices of structural materials were investigated by comparing with those obtained MC calculations as discussed in the next section.

Figure 4.1.2 shows the relative differences in assembly power of the VARIANT solution obtained with the 33-group cross sections of AMPX/SCALE from the MCNP6 solution. As shown in the figure, the VARIANT assembly power agrees very well with the MCNP solution within a maximum difference of 0.342%.

Table 4.1.1 Isotopic composition of mini core problem

Region (Temp)	Isotope	Number Density	Isotope	Number Density
Fuel (900K/600K)	U^{234}	5.13277E-09	Na^{23}	7.14761E-03
	U^{235}	1.35393E-04	Fe^{57}	3.42850E-04
	U^{236}	8.63253E-07	Fe^{58}	4.56271E-05
	U^{238}	8.49024E-03	Ni^{58}	6.79127E-05
	Np^{237}	1.71752E-06	Ni^{60}	2.61598E-05
	Pu^{236}	8.22000E-12	Ni^{61}	1.13725E-06
	Pu^{238}	5.66109E-07	Ni^{62}	3.62524E-06
	Pu^{239}	4.06653E-03	Ni^{64}	9.23766E-07
	Pu^{240}	2.20870E-04	Cr^{50}	1.04529E-04
	Pu^{241}	1.44905E-05	Cr^{53}	2.28569E-04
	Pu^{242}	1.03603E-06	Cr^{54}	5.68956E-05
	Am^{241}	6.35730E-07	Mn^{55}	1.06578E-04
	Am^{42M}	1.27403E-08	Mo^{92}	8.16904E-05
	Am^{243}	2.74440E-08	Mo^{94}	5.09188E-05
	Cm^{242}	2.10659E-08	Mo^{95}	8.76355E-05
	Cm^{243}	3.31710E-10	Mo^{96}	9.18188E-05
	Cm^{244}	2.16128E-09	Mo^{97}	5.25702E-05
	Cm^{245}	8.52965E-11	Mo^{98}	1.32829E-04
	Cm^{246}	1.16828E-12	Mo^{100}	5.30106E-05
	Zr^{91}	3.66150E-04	(600K)	
	Zr^{92}	5.59668E-04	Fe^{56}	1.00000E-02
	Zr^{94}	5.67176E-04	Cr^{52}	1.00000E-02
	Zr^{96}	9.13743E-05		
	(900K)			
Reflector (600K)	Na^{23}	3.49766E-03	Mo^{92}	6.14180E-05
	Fe^{57}	1.24758E-03	Mo^{94}	3.82828E-05
	Fe^{58}	1.66029E-04	Mo^{95}	6.58878E-05
	Ni^{58}	2.47122E-04	Mo^{96}	6.90332E-05
	Ni^{60}	9.51908E-05	Mo^{97}	3.95244E-05
	Ni^{61}	4.13788E-06	Mo^{98}	9.98663E-05
	Ni^{62}	1.31934E-05	Mo^{100}	3.98555E-05
Barrel (600K)	Na^{23}	1.94217E-03	Ni^{62}	4.75903E-06
	B^{10}	8.19022E-03	Mo^{92}	2.21543E-05
	B^{11}	3.29663E-02	Mo^{94}	1.38091E-05
	Na^{23}	3.85752E-03	Mo^{95}	2.37666E-05
	Fe^{57}	4.50017E-04	Mo^{96}	2.49012E-05
	Fe^{58}	5.98890E-05	Mo^{97}	1.42570E-05
	Ni^{58}	8.91401E-05	Mo^{98}	3.60231E-05
	Ni^{60}	3.43366E-05	Mo^{100}	1.43764E-05
	Ni^{61}	1.49259E-06		

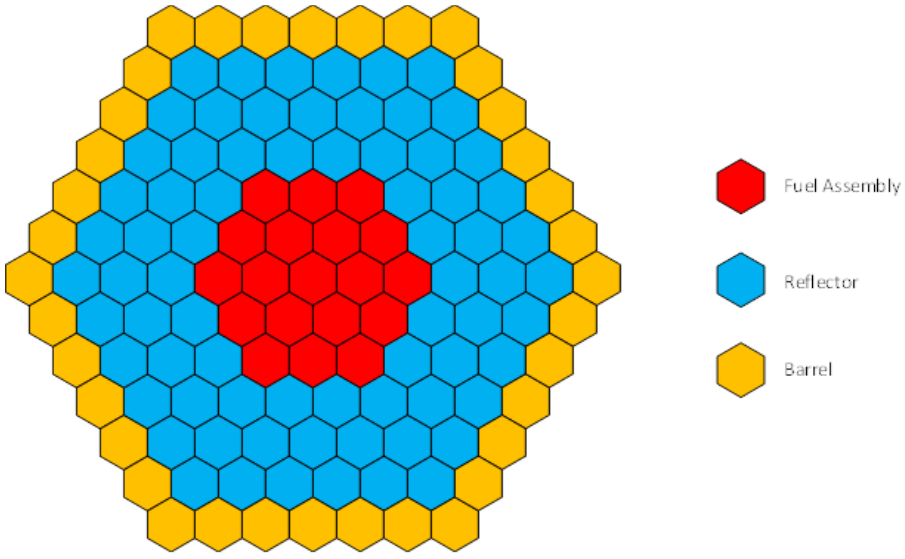

Figure 4.1.1 Configuration of mini core benchmark problem

Table 4.1.2 Eigenvalues of 33-group MG-KENO for mini core problems

Scattering order	Multiplication factor (k_{inf})					Remark
	MCNP	VARIANT (MC^2-3)	Δk (pcm)	VARIANT (AMPX /SCALE)	Δk (pcm)	
P1	1.16322 (10)	1.42416	-12,504	1.42623	-12,555	w/o Fe^{56} and Cr^{52}
P3		1.00344	-2,120	1.00352	-2,314	
P5		1.16188	-134	1.15998	-324	
P5	1.26702 (10)	1.26509	-193	1.25812	-890	w/ Fe^{56} and Cr^{52}

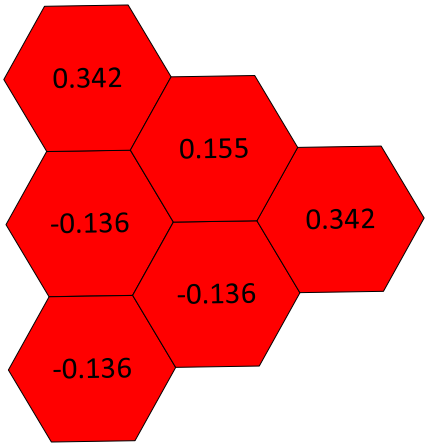

Figure 4.1.2 Relative difference (%) in assembly power density between MCNP6 and DIF3D/VARIANT with 33-group AMPX/SCALE cross section (60˚ rotational symmetry)

4.2 PROBLEMS OF STRUCTURAL MATERIAL CROSS SECTIONS

The benchmark calculations in Section 4.1 showed that there might be significant errors in structural material cross sections and scattering matrices, even though the assembly power shows good agreement with the MCNP result. In order to investigate the accuracy of cross sections and scattering matrices of structural materials, AMPX/SCALE 33-group cross sections and scattering matrices were compared to the reference results obtained from a CE MC calculation with the McCARD code [Shi12].

Figure 4.2.1 compares the 33-group AMPX total cross section of Na^{23}, Cr^{52} and Fe^{56} with the McCARD results. The cross section error plot shows noticeable errors in Cr^{52} cross sections in the energy rage from 10^4 to 10^6 eV, where broad resonances of Cr^{52} and Fe^{56} exist. Furthermore, Zr^{90} also has a similar problem at the vicinity of lower boundary of URR as described in Section 3.1 in relation to the ABTR pin cell problem. Figure 4.2.2 compares the Zr^{90} absorption cross sections of MCNP and MG-KENO. The relative error in the collapsed 252-group Zr^{90} absorption cross section is 68% around 100 keV, which is the lower boundary of the URR of ZR^{90}. Since Na^{23} and Fe^{56} also have broad resonances in this energy range and does not show similar errors, it is likely that the AMPX resonance cross section tables for Zr^{90} and Cr^{52} were not properly generated and needs to be addressed in the future.

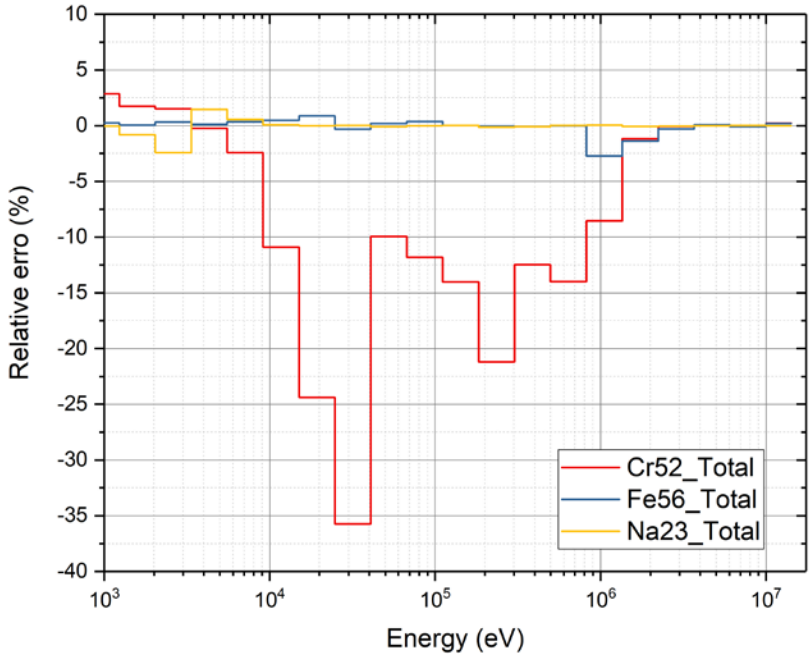

Figure 4.2.1 Total Cross Section differences of Na^{23}, Cr^{52} and Fe^{56} between AMPX/SCALE and McCARD for mini core problem

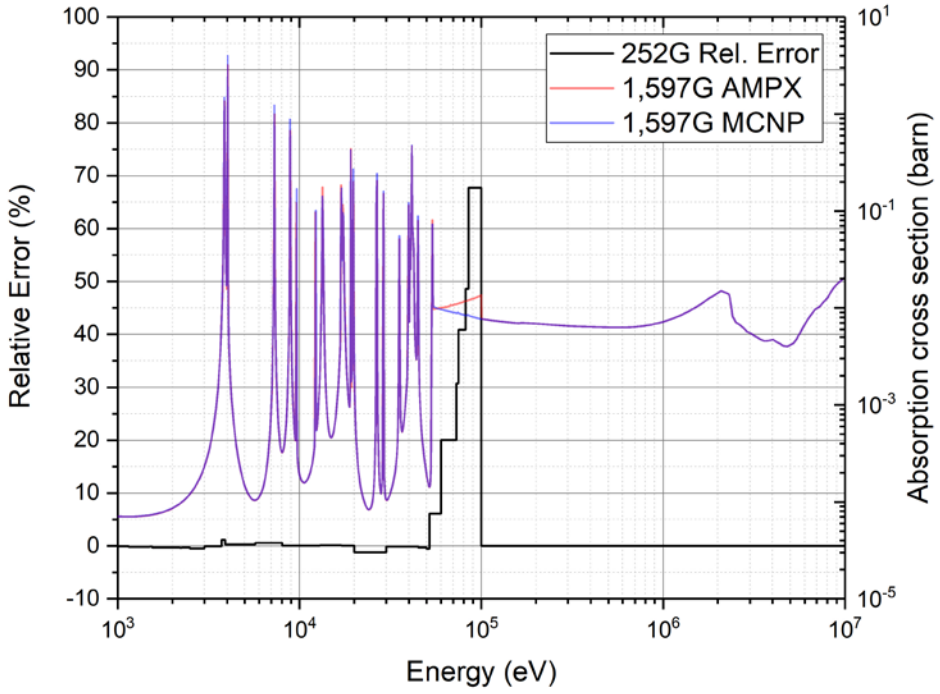

Figure 4.2.2 Comparison of absorption cross section of Zr_{90} between AMPX/SCALE and MCNP for ABTR pin cell problem

Figures 4.2.3 and 4.2.4 also compare the P_0 and P_1 scattering matrices of the 33-group AMPX cross sections of Fe^{56} with the corresponding scattering matrices from the McCARD calculation. It can be seen that P_0 scattering matrix generally agrees well with the McCARD result. It is noted that the huge errors in some off-diagonal elements are due to the large relative uncertainties of tallied MC solutions. However, large relative errors (>50%) are observed at the vicinity of diagonal elements of P_1 scattering matrix, which lead to the notable discrepancies in the k_∞ difference in Table 4.1.2. It is reported that the AMPX MG library has an issue in higher order scattering cross sections in the fast energy range [Kim17]. It is also noted that McCARD generates higher order scattering matrices using the scalar flux, which can be attributed to the above errors. Thus, further investigation is required to identify the root cause of differences in cross sections and scattering matrices.

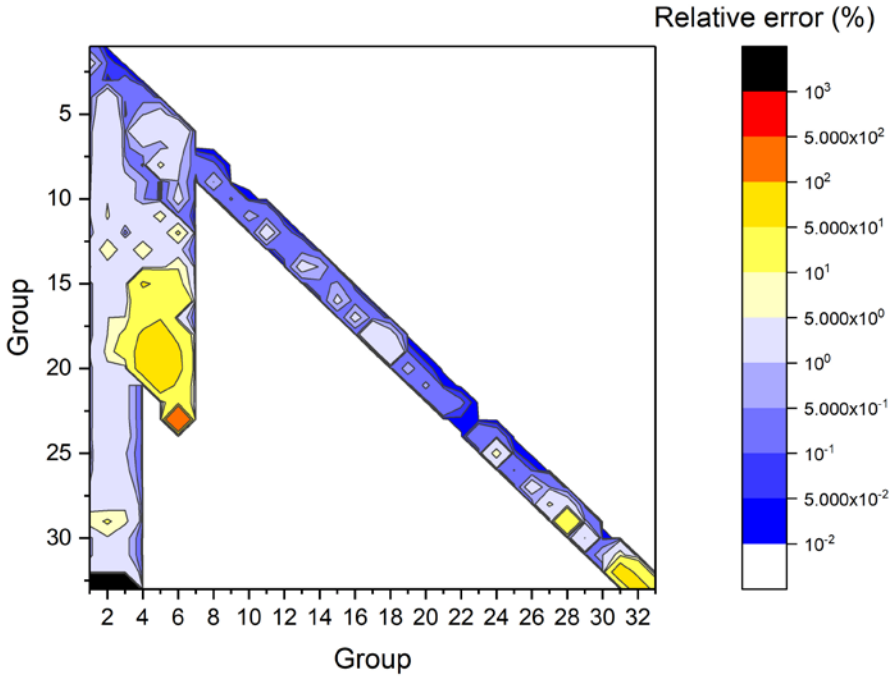

Figure 4.2.2 Comparison of P_0 scattering matrix of Fe^{56} between AMPX/SCALE and McCARD for ABTR mini-core problem

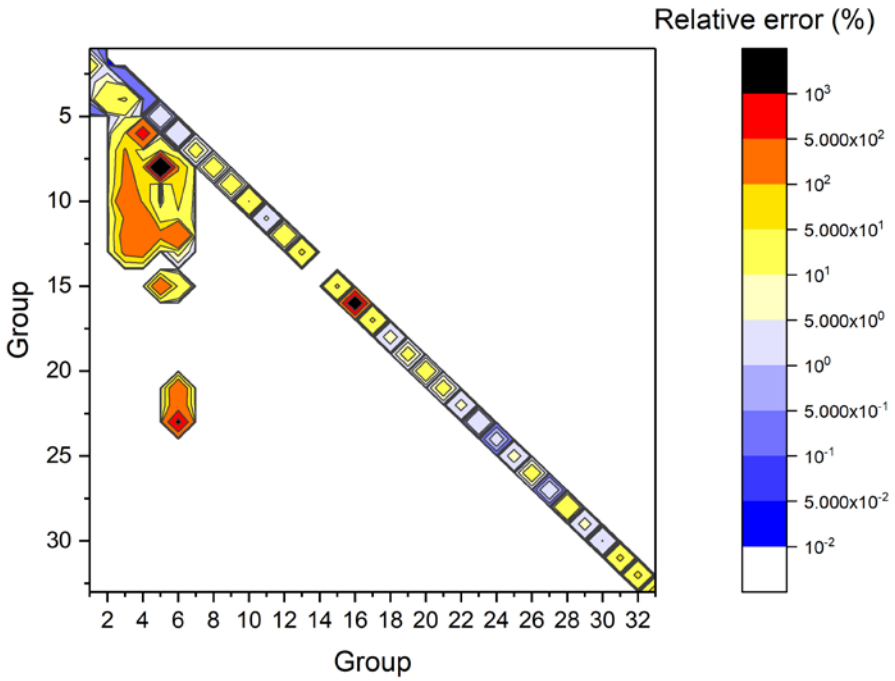

Figure 4.2.2 Comparison of P_0 scattering matrix of Fe^{56} between AMPX/SCALE and McCARD for ABTR mini-core problem

5. CONCLUSION

A 1,597-group AMPX cross section library has been generated using AMPX/SCALE MG procedure to overcome the limitations of the current 252-group AMPX library for the highly voided BWR and fast reactor applications. Despite of remarkable accuracy improvements in reaction rates and reactivity using the 1,597-group library, a lattice calculation with 1,597-group library is extremely time consuming. To improve the computational efficiency without loss of accuracy, a two-step UFG lattice calculation procedure has been proposed and implemented in the SCALE code package. Several internal collapsing procedures with different transport solvers (e.g., 0D slowing down, 2D NEWT, and 2D FDM solvers) have been tested against the reference CE MCNP and 1,597-group MG-KENO results. It was found that the resulting 252-group cross sections collapsed with the calculated UFG spectrum yield the same accuracy for BWR and fast reactor pin cell problems as the 1,597-group KENO results. For example, for a 90% voided BWR pin cell problem, a reactivity errors of -28 pcm and -20 pcm were observed when the collapsed 252-group cross sections were determined with the 0D slowing down and 2D NEWT transport calculations, respectively. Detailed reaction rate analysis showed that the observed discrepancies in the reaction rates obtained with the original 252-group library are eliminated by using the collapsed 252-group cross sections. A 99% voided 12×12 BWR lattice problem was also examined using the two-step procedure. It was found that the 252-group cross sections collapsed with a 2D FDM calculation could reproduce the 1,597-group results accurately with -19 pcm error in reactivity and 1.242% maximum relative error in power. The two-step UFG lattice calculation also reduced the computing time by a factor of 13 compared to the 1597-group lattice calculation.

In order to extend the capability of AMPX/SCALE library to fast reactor applications, a new fast reactor analysis procedure has been established by adopting the ANL fast reactor analysis procedure. In this procedure, a whole-core transport calculation is performed by using the TWODANT transport code to generate the region dependent broad group cross sections by taking into account the region-to-region spectral transition. A utility program has been developed to covert the AMPX/SCALE library to the ISOTXS format used in TWODANT and to generate the collapsed broad group library for the subsequent DIF3D/VARIANT whole-core calculations. A preliminary test with a simplified ABTR mini-core problem indicated that a new procedure with AMPX/SCALE library can be applicable to fast reactor analysis. However, non-negligible errors were found in the cross sections and scattering matrices of some structure materials such as Zr^{90}, Cr^{52} and Fe^{56}. Further investigation is required to resolve the observed cross section errors in structure materials as well as further verification tests with various benchmark problems.

REFERENCES

[[Aki02] A. Yamamoto, T. Ikehara, et al., "Benchmark Problem Suite for Reactor Physics Study of LWR Next Generation Fuels," vol. 39, no. 8, pp. 900–912 (2002).

[Alc90] R. E. Alcouffe, F. W. Brinkley et al., "User's Guide for TWODANT: A Code Package for Two-Dimensional, Diffusion-Accelerated, Neutral-Particle Transport," LA-10049-M, Los Alamos National Laboratory (1990).

[CAS15] "Consortium for Advanced Simulation of Light Water Reactors (CASL)." URL http://www.casl.gov/ (2015).

[Cha06] Y.I. Chang, P. J. Finck, et al., "Advanced Burner Test Reactor Preconceptual Design Report," ANL-ABR-1, Argonne National Laboratory (2006).

[Cse12] Cross Section Evaluation Working Group, "ENDF-6 Formats Manual, Data Formats and Procedures for the Evaluated Nuclear Data File ENDF/B-VI and ENDF/B-VII," CSEWG Document ENDF-102, National Nuclear Data Center, Brookhaven National Laboratory (2012).

[Jeo18] B. K. Jeon, W. S. Yang, et al., "Development of Ultra-Fine Multi-Group Cross Section Library of the AMPX/SCALE Code Packages, Rev. 0," CASL-U-2018-1507-000, Oak Ridge National Laboratory (2018).

[Kim16] K. S. Kim, "Generation of the V4.2m5 AMPX and MPACT 51 and 252-Group Libraries with ENDF/B-VII.0 and VII.1, Rev. 0," CASL-U-2016-1177-000, Oak Ridge National Laboratory (2016).

[Kim17] K. S. Kim, K. Clarno, et al., "Development of the V4.2m5 and V5.0m0 Multigroup Cross Section Libraries for MPACT for PWR and BWR, Rev. 0," ORNL/TM-2017/95, Oak Ridge National Laboratory (2017).

[Kim18] K. S. Kim, M. Willams, et al., "The AMPX/SCALE multigroup cross section processing for fast reactor analysis," *PHYSOR 2018*, Cancun, Tennessee, Mexico, April 22-26, 2018 (2018).

[Lee11] C. H. Lee and W. S. Yang, "MC^2-3: Multigroup Cross Section Generation Code for Fast Reactor Analysis," ANL-NE-11-41, Argonne National Laboratory (2011).

[Mpa13] MPACT: User's Manual Version 1.0.0, November 8, 2013 (2013).

[Pal95] G. Palmiotti, E. E. Lewis, et al., "VARIANT: VARIational Anisotropic Nodal Transport for Multidimensional Cartesian and Hexagonal Geometry Calculation," ANL-95/40, Argonne National Laboratory (1995)

[Rim95] G, Rimpault, "Algorithmic features of the ECCO Cell Code for treating heterogeneous fast reactor subassemblies," in: International Topical Meeting on Reactor Physics and Computations, Portland, Oregon, May 1-5, 1995. (1995)

[Sca16] "SCALE: A Modular Code System for Performing Standardized Computer Analyses for Licensing Evaluation," ORNL-TM/2005/39, Version 6.2, Oak Ridge National Laboratory, Oak Ridge, Tennessee (2016). (Available from Radiation Safety Information Computational Center at Oak Ridge National Laboratory as CCC-834.)

[Shi12] H. J. Shim et al., "McCARD: Monte Carlo Code for Advanced Reactor Design and Analysis," *Nucl. Eng. Technol.*, **44**, 2, 161 (2012).

[Tak06] T. Takeda, T. Okamote, et al., “Effect of anisotropic scattering in neutronics analysis of BWR assembly,” *Ann. Nucl. Energy.*, **33**, 16, 1315 (2006).

[Tau80] M. Taube, W. Heer., “Reactor with very low fission product inventory,” EIR-Bericht Nr. 411, Swiss Federal Institute of Reactor Technology (1980).

[Tur16] J. Turner et al., “The Virtual Environment for Reactor Applications (VERA): Design and architecture,” *Journal of Computational Physics*, **326**, 544 (2016).

[Wia14] D. Wiarda, S. Goluoglu, M.E. Dunn, N.M. Green and L. M. Petrie, “AMPX-6: A Modular Code System for Processing ENDF/B Evaluations,” in preparation (2014).

[Wil12] Mark L. Williams, Kang-Seog Kim, “The Embedded Self-Shielding Method,” *PHYSOR 2012*, Knoxville, Tennessee, USA, April 15–20, 2012 (2012).

[Yan10] W. S. Yang et al., “Neutronics modeling and simulation of sharp for fast reactor analysis,” *Nucl. Eng. Technol.*, **42**, 5, 520 (2010).

[Yan12] W. S. Yang, “Fast reactor physics and computational methods,” *Nucl. Eng. Technol.*, **44**, 2, 177 (2012).